

High-Resolution Magnetic Resonance Imaging Quantitatively Detects Individual Pancreatic Islets

Smaragda Lamprianou,¹ Riikka Immonen,² Christine Nabuurs,² Asllan Gjinovci,¹ Laurent Vinet,¹ Xavier C.R. Montet,³ Rolf Gruetter,^{2,3,4} and Paolo Meda¹

OBJECTIVE—We studied whether manganese-enhanced high-field magnetic resonance (MR) imaging (MEHFMRI) could quantitatively detect individual islets in situ and in vivo and evaluate changes in a model of experimental diabetes.

RESEARCH DESIGN AND METHODS—Whole pancreata from untreated ($n = 3$), MnCl_2 and glucose-injected mice ($n = 6$), and mice injected with either streptozotocin (STZ; $n = 4$) or citrate buffer ($n = 4$) were imaged ex vivo for unambiguous evaluation of islets. Exteriorized pancreata of MnCl_2 and glucose-injected mice ($n = 6$) were imaged in vivo to directly visualize the gland and minimize movements. In all cases, MR images were acquired in a 14.1 Tesla scanner and correlated with the corresponding (immuno)histological sections.

RESULTS—In ex vivo experiments, MEHFMRI distinguished different pancreatic tissues and evaluated the relative abundance of islets in the pancreata of normoglycemic mice. MEHFMRI also detected a significant decrease in the numerical and volume density of islets in STZ-injected mice. However, in the latter measurements the loss of β -cells was undervalued under the conditions tested. The experiments on the externalized pancreata confirmed that MEHFMRI could visualize native individual islets in living, anesthetized mice.

CONCLUSIONS—Data show that MEHFMRI quantitatively visualizes individual islets in the intact mouse pancreas, both ex vivo and in vivo. *Diabetes* 60:2853–2860, 2011

Despite the high incidence of diabetes, the precise molecular and cellular mechanisms that cause the decrease in the mass and function of the insulin-producing β -cells, observed in both the type 1 and type 2 forms of the disease, remain to be elucidated (1). At present, the only, although somewhat indirect, way to monitor the onset and the evolution of the diseases in a given individual is by using sensitive immunological and functional tests, which require injections and repeated blood sampling. However, we still lack a method that could visualize and quantitate pancreatic β -cells in vivo, in a fully noninvasive way. As a result, we also lack a solid biological basis to target new therapeutic approaches that could promote the regeneration (type 1 diabetes) or

the function (type 2 diabetes) of β -cells. The difficulty in imaging these cells stems from their deep abdominal location, their distribution in small (50–600 μm in diameter) islets of Langerhans, their modest volume density ($\sim 1\%$) in a control pancreas, and their close relationships to different cell types of both endocrine and exocrine nature.

Several of these issues have been partially solved using optical methods, which can now investigate laboratory rodents (2–4), but which cannot be adapted to human studies, given the limited tissue penetration of light (2,4–6). Penetration is not an issue in magnetic resonance (MR) imaging (MRI) and positron-emitting tomography (PET) imaging, which are convenient for human applications, specifically if combined with computed tomography. Because islets are structurally and functionally heterogeneous, and are not all simultaneously altered to the same degree during diabetes development, their individual visualization is important. The choice of an imaging modality is then restricted to MRI, given that the lateral resolution of PET is, at best, in the millimeter range (7). MRI has already been used to visualize transplanted islets (8–11), but has not yet been shown to detect native islets in situ, mostly because of an insufficient spatial resolution, which is only provided by the use of a high magnetic field (8,12–14).

The aim of the current study was to investigate whether imaging of individual islets could be achieved using a 14.1 Tesla (T) MR scanner. In the absence of a validated probe for the specific staining of β -cells, we have also tested whether the MRI contrast of these islets could be enhanced by an in vivo infusion of manganese (12). Our data document that the combination of these conditions, in manganese-enhanced high-field magnetic resonance imaging (MEHFMRI), allows for the easy differentiation of multiple tissues within the whole murine pancreas, including individual islets of Langerhans. The approach quantitatively detects the loss of pancreatic islets in an animal model of type 1 diabetes, and with this approach pancreatic islets in the living animal can be investigated.

RESEARCH DESIGN AND METHODS

Animals. C57BL6 mice were used throughout. All animals were anesthetized with an intraperitoneal injection of 1 g/kg body weight (b.w.) pentothal. Three mice were immediately killed. Five mice had a polyethylene (PE50) catheter with an adapted tip (Eppendorf, 0030 001.222) inserted into a femoral vein. Through this catheter, a 15 mmol/L MnCl_2 solution (in 0.9% NaCl) was infused at the rate of 4 mL/h for 7 min, using a precision syringe pump. This provided for a cumulative dose of 47 mg of MnCl_2 /kg b.w. Six other mice were given 0.8 g glucose/kg b.w. i.p. once, 15 min before the start of the manganese infusion. After 30 min of the manganese infusion, the animals were again injected intraperitoneally with 1.7 g glucose/kg b.w., to acutely stimulate the β -cells, and the pancreata were dissected 15 min later.

Four mice were injected intraperitoneally with 200 mg/kg b.w. streptozotocin (STZ; Sigma), whereas four received only the citrate buffer (CB), which was used as a vehicle of the drug. Two weeks later, the mice were anesthetized with 1.5% isoflurane and had two intraperitoneal catheters placed for administration

From the ¹Department of Cell Physiology and Metabolism, University of Geneva, Geneva, Switzerland; the ²Laboratory for Functional and Metabolic Imaging, Ecole Polytechnique Fédérale de Lausanne, Lausanne, Switzerland; the ³Department of Radiology, University of Geneva, Geneva, Switzerland; and the ⁴Department of Radiology, University of Lausanne, Lausanne, Switzerland. Corresponding author: Smaragda Lamprianou, smaragda.lamprianou@unige.ch. Received 26 May 2011 and accepted 10 August 2011.

DOI: 10.2337/db11-0726

This article contains Supplementary Data online at <http://diabetes.diabetesjournals.org/lookup/suppl/doi:10.2337/db11-0726/-/DC1>.

© 2011 by the American Diabetes Association. Readers may use this article as long as the work is properly cited, the use is educational and not for profit, and the work is not altered. See <http://creativecommons.org/licenses/by-nc-nd/3.0/> for details.

of 35 mg/kg b.w. $MnCl_2$ dissolved in N,N-Bis(2-hydroxyethyl)glycine (BICINE) buffer together with 1.5 g/kg b.w. glucose. Both $MnCl_2$ and glucose were manually injected via the catheters, while the animals were inside the magnet bore of the MRI equipment as follows: first, half of the $MnCl_2$ dose (~ 1.5 mL) was injected. After 25 min, all glucose and the second half of the $MnCl_2$ solution were injected. The animals were killed 2 h later, and pancreata were dissected and fixed.

Pancreas processing. At the end of each experiment, the entire pancreas was rapidly dissected as one piece and placed in perfluoropolyether (Fomblin) within a sealed plastic bag. Some pancreata were imaged fresh, immediately after the sampling. Others were fixed for 15 h in 4% paraformaldehyde (PFA) at 4°C, washed in phosphate buffer, and placed individually into a Fomblin-containing bag.

MRI. Ex vivo pancreata were imaged within the Fomblin-containing bags, using a 14.1 Tesla 26 cm horizontal bore scanner (Varian/Magnex Scientific, Abingdon, U.K.) with a 12 cm inner-diameter gradient (400 mT/m in 200 ms, minimized eddy currents), interfaced with a DirectDrive console (Varian, Palo Alto, CA) and a quadrature half-volume coil of 20 mm diameter. High-resolution images were acquired using a gradient echo multislice sequence with fourteen 0.3-mm-thick slices, field of view (FOV) 26*25 mm, and data matrix 512*512 (51*49*300 μm resolution) to cover the whole mouse pancreas. T1/T2* weighted images with repetition time (TR) = 282 ms, echo time (TE) = 7 ms, flip = 60°, and 30 averages were acquired for optimal tissue contrast in a 1 h 12 min acquisition time.

In vivo MRI was performed on externalized pancreata of six mice. Animals were injected intraperitoneally with 35 mg/kg b.w. $MnCl_2$ (dissolved in BICINE buffer) and 1.5 g/kg b.w. glucose 2 to 3 h before anesthesia with 1 to 2% isoflurane in a 3:2 air/O₂ gas mixture. The abdomen was opened, and the spleen was pulled out with the pancreas. The gland was secured to a Plexiglas plate (Supplementary Fig. 1) using a plastic pin inserted between the pancreatic tail and the spleen without damaging the pancreas vessels. Once the plastic pin had been attached to a Plexiglas plate, the pancreas led on a semiflexible plastic support to minimize its movements (Supplementary Fig. 1) and was positioned in the center of a quadrature coil. The whole mounting was placed within 5 min in the MRI equipment, in which the mouse was kept under ventilation, anesthesia, and warmed by water circulation to maintain the body temperature between 35° and 37°C. High-resolution images were acquired using a gradient echo multislice sequence with 14 coronal 0.2-mm-thick slices, FOV 26*26 mm, data matrix 382*382 (68*68*200 μm resolution), and 10 averages. To prevent inference of respiratory movements, images were acquired by gating on the breathing cycle and recorded with TR ~ 700 ms, TE = 5 ms, and flip = 60° in ~ 1 h.

Histology. After in vivo MRI, pancreata were fixed in Bouin's fixative solution (14 g/L of picric acid, 8% formol, and 4% acetic acid) for at least 48 h. All pancreata were washed, dehydrated, and embedded in paraffin, keeping the same orientation that was used during MRI acquisition. Serial sections of 5 μm thickness were cut through the MRI imaged samples, stained with hematoxylin-eosin, digitized using a MIRAX MIDI slide scanner (Zeiss), and analyzed using the MIRAX Viewer software.

Sections from ex vivo imaged pancreata were sequentially passed into Neoclear, twice for 5 min, and then in 100 (twice), 95, 70, 50, and 30% ethanol for 3 min each. The sections were incubated for 1 h in 10 mmol/L NH_4Cl in PBS to remove PFA excess, followed by 30 min in a 0.5% BSA solution in PBS. Sections were stained with either antiglucagon mouse antibody (Sigma) diluted 1/40,000 or anti-insulin guinea pig antibody (Ventrex 675) diluted 1/2,000, for 2 h at room temperature. Thereafter, sections were incubated with donkey anti-mouse fluorescein isothiocyanate (1/400; P.A.R.L.S.) and goat anti-guinea pig-Alexa 488 (1/500; Molecular Probes), respectively, for 1 h at room temperature. Sections were counterstained with 0.03% Evans Blue, coverslipped, and scanned using the MIRAX equipment, operated under ultraviolet rays illumination.

Quantitative analysis. MRI images were analyzed using Matlab R2008a (Math-Works, Natick, MA). The entire pancreas profile and all detectable hyperintense, putative islet-like structures were manually outlined. These regions of interest were used to determine the location, size, shape, number, cross-sectional area, volume, and relative signal intensity.

Sections (5 μm thick) of the same pancreas that had been imaged by MR were stained with hematoxylin-eosin, scanned, and quantitatively evaluated with the MIRAX Viewer software, for evaluation of islet size, volume, and numerical density.

Statistics. Values are shown as means + SEM and were compared using unpaired *t* tests as provided by SPSS (Chicago, IL). Because of the skewed distributions, islet sizes were compared using the nonparametric Mann-Whitney and Kolmogorov-Smirnov tests, also provided by SPSS.

RESULTS

Ex vivo MRI of the intact mouse pancreas. MRI (14.1T) was used to image the entire mouse pancreas in slices of 300 μm thickness and with a 50 μm in plane resolution.

In the absence of a contrast agent, the images showed the lobular structure of the gland (Fig. 1A and Supplementary Fig. 2) and, within these lobules, occasional round-ovoid whitish bodies that corresponded in shape, size, and distribution to putative individual islets (Fig. 1B and Supplementary Fig. 2). Other, much larger structures were located between the pancreatic lobules (Fig. 1C). After infusion of manganese and injection of a glucose dose known to stimulate β -cells, the contrast of the lobular and interlobular structures was enhanced (Fig. 1C and Supplementary Fig. 2).

Histology validates the pancreas substructures imaged by MRI. To positively identify the pancreas structures seen by MRI, we processed each pancreas for histology and screened the sections that were the closest to the plane of the MRI image recorded within the 300- μm -thick tomographic slice of the samples (Figs. 1C and 2A). The presence in both images of ducts and vessels, as well as non-pancreatic tissues, helped precisely match the MRI and the histological images. This procedure confirmed the different appearance of the pancreas and close-by organs (such as spleen or intestines) and differentiated, within the gland, the lymphatic ganglia from the adjacent exocrine tissue (Fig. 1C). Moreover, higher magnification views of both MR images and corresponding histological sections confirmed that the small, round-ovoid structures scattered within the exocrine pancreas were bona fide pancreatic islets of Langerhans (Fig. 2A). In the MRI images of pancreata from mice that had not been infused with manganese, islets were also occasionally visible as hyperintense whitish bodies (Fig. 1B). However, the intensity of the islet signal, relative to that of the adjacent exocrine pancreas, was somewhat higher ($P < 0.001$, $n = 27$) after manganese infusion than in the noninfused controls (Fig. 2B).

Quantification of the islet mass by MRI. To compare the size of putative islets as well as their numerical and volume densities within the pancreas, the entire pancreata of five animals that had received both manganese and glucose were evaluated first by MRI and then by histology (Fig. 3A). Morphometry showed the expected asymmetrical distribution of islet sizes in histological sections (Fig. 3B). The size distribution determined by the MRI was significantly ($P < 0.001$) shifted to higher diameters, likely a result of partial volume effects of the 300 μm slice thickness, which made the detection of islets < 50 μm in diameter difficult (Fig. 3B). Despite this limitation, MRI evaluated that the volume density of islets, i.e., the relative volume of islets within the pancreas, was on the average $0.8 \pm 0.2\%$ ($n = 5$; Fig. 3C). The average numerical density of islets was 1.2 ± 0.3 per mm^3 of pancreas ($n = 5$).

To evaluate whether the loss of islets in an animal model of type 1 diabetes can be detected by MRI, we injected mice intraperitoneally with either 200 mg/kg b.w. STZ or an equivalent volume of the CB (sham treatment), which was used as vehicle for the drug (Fig. 4A). Two weeks after the STZ injections MRI evaluation showed that the hyperglycemic mice (Supplementary Table 1) had a pancreas volume (V_p ; bottom panel of Fig. 4B) that was not significantly different from that of the citrate-injected controls. In contrast, the relative number (N_v ; top panel of Fig. 4B) and volume density (V_v ; middle panel of Fig. 4B) of the islets were decreased by 55% ($P < 0.01$) and 45% ($P < 0.001$), respectively, in the STZ-injected mice (Fig. 4B). These changes were confirmed by the histological analysis of the same pancreas (Fig. 4A). Given that the hyperglycemia of the STZ-injected mice (Supplementary Table 1)

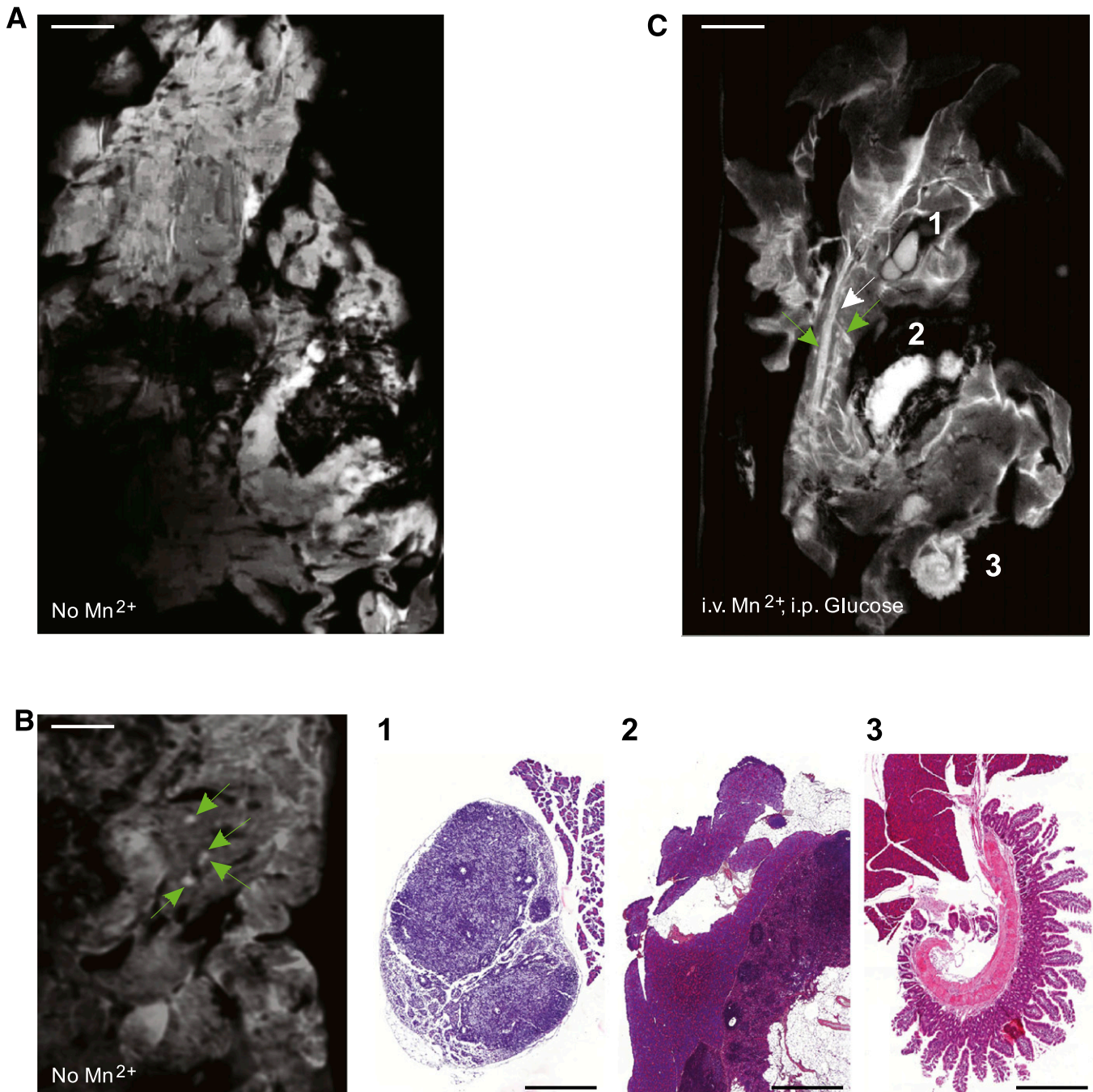


FIG. 1. High-resolution MRI reveals the structure of the entire mouse pancreas. *A* and *B*: Whole mouse pancreata (300- μ m-thick slices) were imaged ex vivo, with 50 μ m in plane resolution (TR/TE = 282/7 ms). *A*: In an image obtained without contrast agent, pancreatic lobules are seen, most of which feature a somewhat homogeneous and structureless content at this low magnification. Scale bar: 1 mm. *B*: Under these conditions, MRI infrequently identified putative islets of Langerhans (green arrows) within the intact pancreas. Scale bar: 1 mm. *C*: The contrast of pancreatic lobules was enhanced after intravenous infusion of $MnCl_2$ combined with an intraperitoneal injection of glucose. Under these conditions, MRI allowed to distinguish whitish tubular structures, as well as highly contrasted round-ovoid structures of various sizes. The smallest of these structures (<0.5 mm; green arrows) was observed within the pancreatic lobules. Larger structures (>1 mm) were seen between the lobules. The latter structures were identified by histological analysis of the very same pancreas, confirming that MRI differentiates the pancreatic parenchyma from intrapancreatic lymphatic ganglia (*C1*), spleen (*C2*), and loops of small intestine (*C3*). Scale bar: 1 mm in *A–C*; 0.5 mm in lower panels *B1–3*. (A high-quality digital representation of this figure is available in the online issue.)

suggested a more profound drop of the insulin-producing β -cells, we immunostained the pancreas for insulin and glucagon (Fig. 4C). As expected, we found that the islets of the STZ-injected mice contained much less insulin-containing β -cells than those of controls. However, anti-glucagon staining demonstrated an increased number of glucagon-containing α -cells (Fig. 4C). In some cases, the latter cell

type occupied almost the entire surface of the small, residual islets (Fig. 4C).

Visualization of islets by Mn^{2+} -enhanced MRI in living mice. To determine whether high-field MRI can detect islets in vivo, the pancreas was exteriorized through an abdominal incision, without affecting its normal blood flow and innervation (Supplementary Fig. 1). This externalization

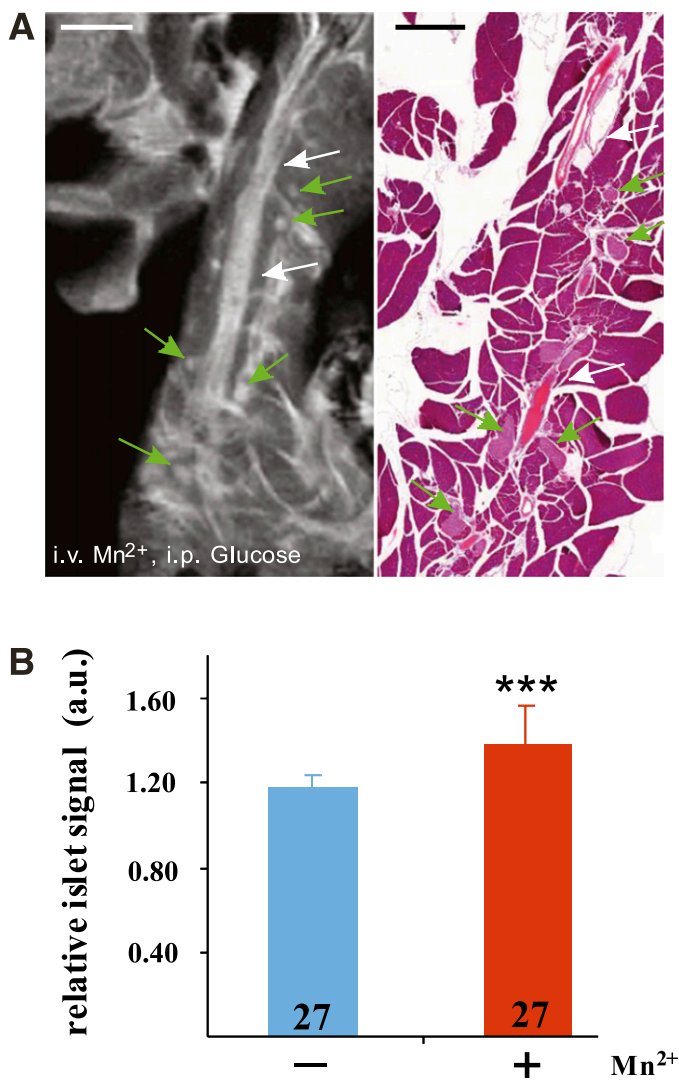


FIG. 2. Individual pancreatic islets are visualized by MRI. **A:** This MR image (*left*) is a high magnification view of the pancreas shown in Fig. 1C, recorded with a 50 μm in plane resolution. Small, round-ovoid whitish structures (several are pointed by green arrows) are seen dispersed within the pancreatic lobules. Histology (*right*) confirmed that these structures are pancreatic islets of Langerhans, dispersed within the exocrine parenchyma, between vessels and ducts (white arrows). Scale bar: 1 mm. **B:** Quantification of the islet signal intensity, relative to that of the surrounding exocrine tissue, confirmed that the MR image of islets was more contrasted ($***P < 0.001$) in the Mn^{2+} -infused mice (red bar) than in noninfused controls (blue bar). Values are means + SEM of the number of islets indicated within the columns. a.u., Arbitrary units. (A high-quality digital representation of this figure is available in the online issue.)

minimized the effects of breathing and bowel movements on imaging and allowed for the unambiguous identification of the pancreas, which is not immediate in the noninvasive imaging of mice. Under these conditions, MRI revealed intrapancreatic structures similar to those observed in the ex vivo samples, including putative pancreatic islets of Langerhans, which appeared as intralobular whitish bodies (Fig. 5). Correlative histology confirmed that these bodies were bona fide islets (Fig. 5).

DISCUSSION

Imaging the pancreatic islets, which comprise all insulin-producing β -cells of our body and most of its glucagon-producing α -cells, is urgently needed to progress in our

understanding of the natural history and the pathophysiology of diabetes, as well as to monitor candidate treatments aimed at compensating and improving, if not curing, the disease (15,16). Although progress has been made in the imaging of transplanted islets, which can be labeled before transplantation (8–11,17,18), the imaging of the native islets within an entire, intact pancreas still raises significant challenges. This is because of the small size of pancreatic islets, their scattering within the pancreas, their poor contrast relative to that of the surrounding tissues, and the deep position of the pancreas within the abdomen. In laboratory mice, at least some of these challenges can be solved using β -cell-specific probes and near-infrared optical methods (19). However, in larger animals and in humans, the use of nonoptical methods, such as PET or MRI, is required, because of the limited tissue penetration of light (15,16,20,21). If PET has a unique sensitivity and is quantitative, it lacks the resolution to differentiate individual islets, and its application to large numbers of individuals is complicated by the need to generate positron-emitting isotopes, the short half-life of these compounds, and a variety of safety issues. MRI is of more widespread applicability, but questions arise as to whether it could visualize the small pancreatic islets, which in a control human pancreas represent all together no more than 1 g wet weight tissue, and, furthermore, whether it is amenable to a sound quantitative analysis of their mass and function (15,16,21,22).

Using the increased sensitivity of a 14.1T MRI system, we achieved a spatial resolution (23) that, on theory, should be sufficient to detect islets. Using a correlative MRI-histology approach, we document here that the technique indeed visualizes individual islets within a whole, fresh, and untreated mouse pancreas, after either excision of the gland or its externalization in a living mouse. We further document that the islet visualization is enhanced by the prior vascular infusion of manganese (12,14,24,25), particularly in animals challenged with an acute glucose load, since the cation accumulates in islet cells during stimulation of insulin secretion (12,14,24). The study provides evidence that a clinically relevant imaging methodology can be adapted to image individual pancreatic islets in the intact rodent pancreas.

Our study further shows that the analysis of MEHFMRI images provides a sound estimate of the islet mass in control mice. Thus, both the numerical and volume density estimates of the endocrine islets were consistent with the many previous reports, which evaluated these parameters by morphometry of histological sections (26–30). However, the volume and number of the islets were underestimated by MEHFMRI, presumably as a result of the so-called partial volume effect (31,32), as small islets (<50 μm in diameter), which represent but a small proportion of the total β -cell volume, escaped MRI detection within the 300- μm -thick pancreas slices that we imaged. Our study also provides evidence that MRI can quantitate a partial loss of islets, as a result of a major cytotoxic insult to β -cells. Thus, 2 weeks after administration of a dose of STZ, which made the animals stably and overtly hyperglycemic, MRI revealed a 45–55% loss in the volume and numerical densities of the endocrine islets. Immunolabeling of the same pancreas showed that, as expected from many previous reports (31–40), the loss of β -cells was sizably larger than suggested by this percentage and was associated to the persistence of many glucagon-containing α -cells (38,41). Thus, under the conditions we used, MRI did not differentiate the islets

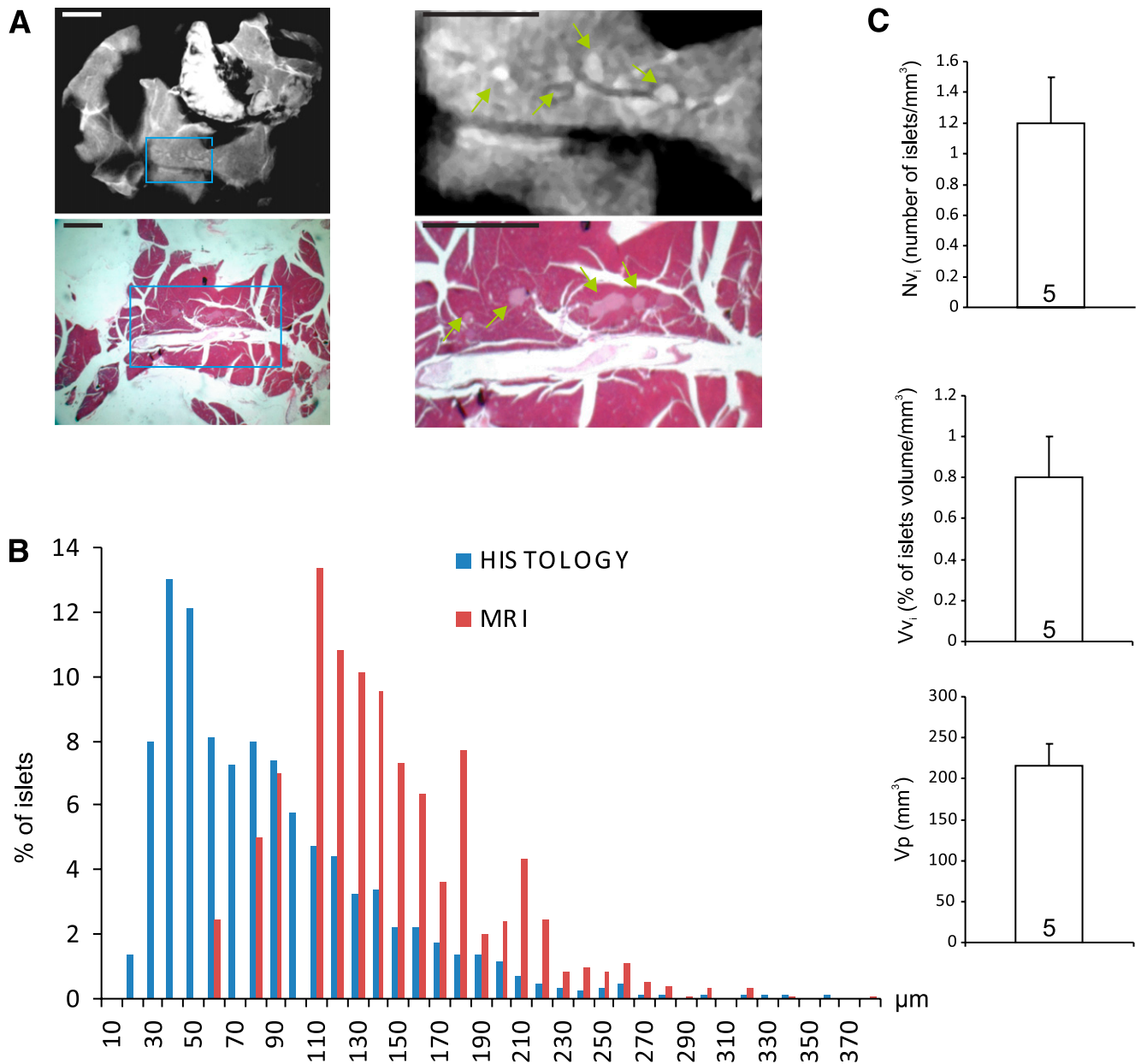


FIG. 3. MRI quantifies islet mass and size. **A:** Islets of different sizes were detected in the MR images of whole mouse pancreas (*top*) and confirmed by correlative histology (*bottom*). The *right panels* are enlargements of the regions boxed in the *left panels*. Scale bar: 1 mm. **B:** Islet sizes were measured in both MR and histology images. The distribution of the values was asymmetrical in both cases, confirming that islets $<150 \mu\text{m}$ in diameter predominate in the control mouse pancreas, whereas islets $>300 \mu\text{m}$ are rare. Of note, islets $<50 \mu\text{m}$ in diameter escaped MRI detection. **C:** Further morphometric evaluation of MR images showed that MRI detected on the average 1 islet/ mm^3 of pancreas (*left*), accounting for a relative volume of the endocrine micro organs of $0.8 \pm 0.2\%$ (*middle*). A mean of 268 islets per animal ($n = 5$) was detected; V_{v_i} , volume density of the islets (Ni/mm^3 of pancreas); V_p , total volume of pancreas analyzed (mm^3). Values are means + SEM of five control mice. (A high-quality digital representation of this figure is available in the online issue.)

containing residual β -cells from those predominantly made of α -cells, most likely because manganese is taken up by multiple pancreatic cell types, including α -cells (42,43). These considerations raise concerns that MEHF MRI may not be adequate to detect the modest loss in β -cell mass that may progressively take place over months of diabetes development, nor the even more modest increase in β -cell numbers, which could be anticipated under conditions of spontaneous or treatment-induced β -cell proliferation, transdifferentiation, or neogenesis. To increase the sensitivity of the approach, the development of ligands specifically targeting β -cells (19) is most needed. With the availability of such ligands, MRI may become useful for the

evaluation and longitudinal monitoring of both type 1 and type 2 diabetes (4,44–47).

Given the present methodological stage of these experiments, we focused on the MRI of islets in either ex vivo or exteriorized mouse pancreas. The obvious next step is to test whether the approach is amenable to the quantitative imaging of native islets, under noninvasive, in vivo conditions. This question raises significant challenges. First, an in vivo MRI should take into consideration the circulatory, respiratory, and intestinal movements of the living animal, which cyclically displace the islets by a factor significantly larger than their average diameter. To compensate for these movements, the image acquisition needs to be

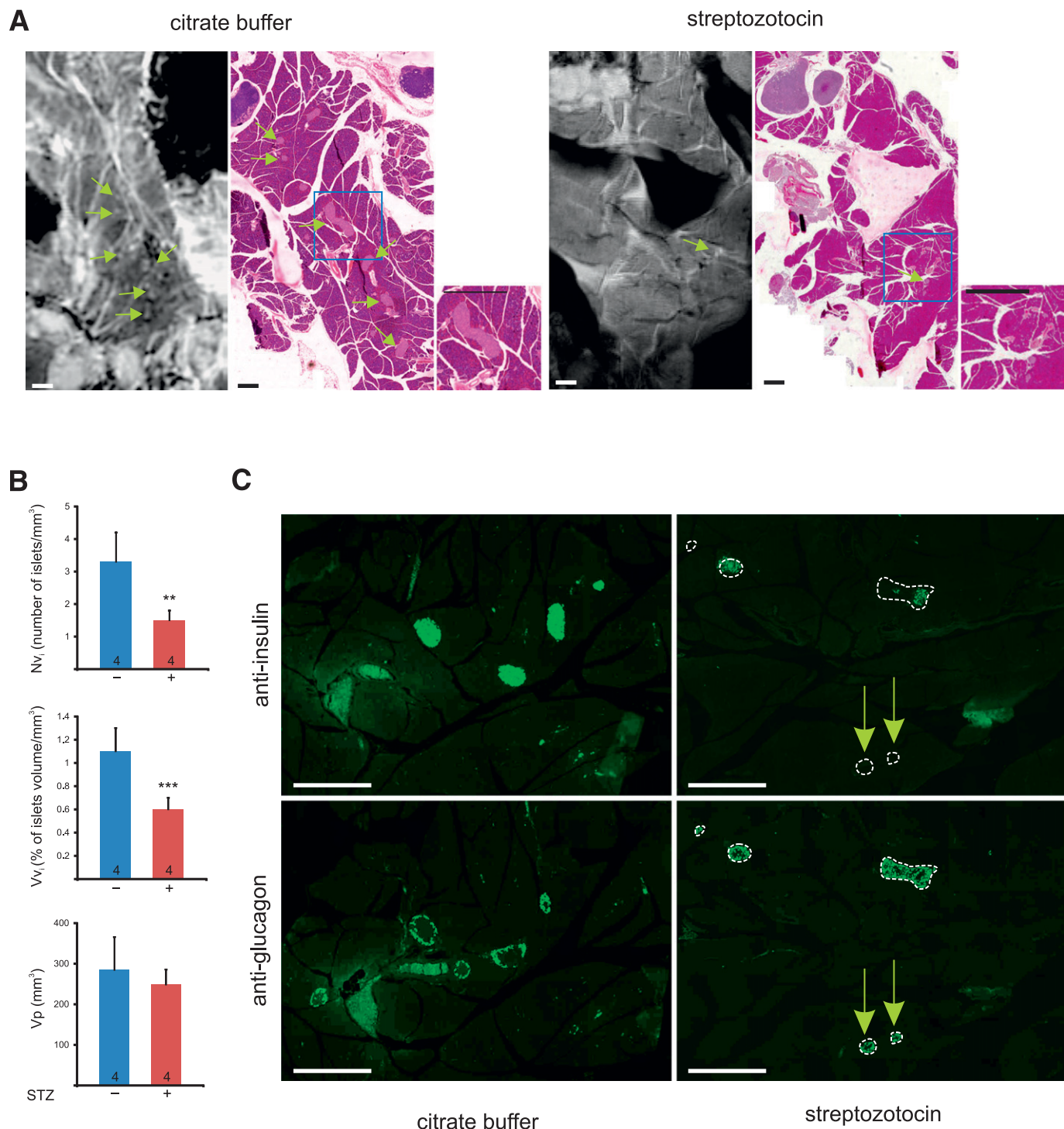


FIG. 4. MRI detects the loss of islets in a diabetic mouse model. **A:** High magnification MR and histology images of pancreas from mice injected with either CB (normoglycemic controls) or the buffer supplemented with STZ (hyperglycemic mice). Whitish (MRI)/pink islets (histology) were seen more frequently in the pancreata of control rather than of STZ-injected mice (some islets are pointed by green arrows). Scale bar: 1 mm and 0.5 mm in the insets. **B:** Morphometric analysis of the MR images showed that hyperglycemic mice had a pancreas volume (V_p ; *bottom*) that was not significantly different from that of the citrate-injected controls. In contrast, the relative number (N_v ; *top*) and volume density (V_v ; *middle*) of the islets were decreased by 55 and 45%, respectively, in the STZ-injected mice. Data are mean + SEM of the indicated number of pancreas (** $P < 0.01$; *** $P < 0.001$). **C:** Immunostainings of consecutive pancreas sections of control and STZ-treated mice with antibodies against insulin and glucagon show that the STZ treatment significantly reduced the number of β -cells in most islets (outlined by white dotted lines). Most islets still contained many glucagon-containing α -cells. Some small islets (arrows) were essentially made by the latter type of islet cells and were fully devoid of insulin-containing cells. Scale bar: 0.5 mm. (A high-quality digital representation of this figure is available in the online issue.)

synchronized with the breathing and beating cycles, which is achievable with modern equipment. Second, a major limitation of pancreas MRI in the living rodent results from the small size of the gland and its intricate topography with

respect to the other abdominal organs. The MRI definition of the rodent pancreas is therefore cumbersome and, to some extent, ambiguous. A solution to this problem awaits the development of a second, still putative ligand labeling

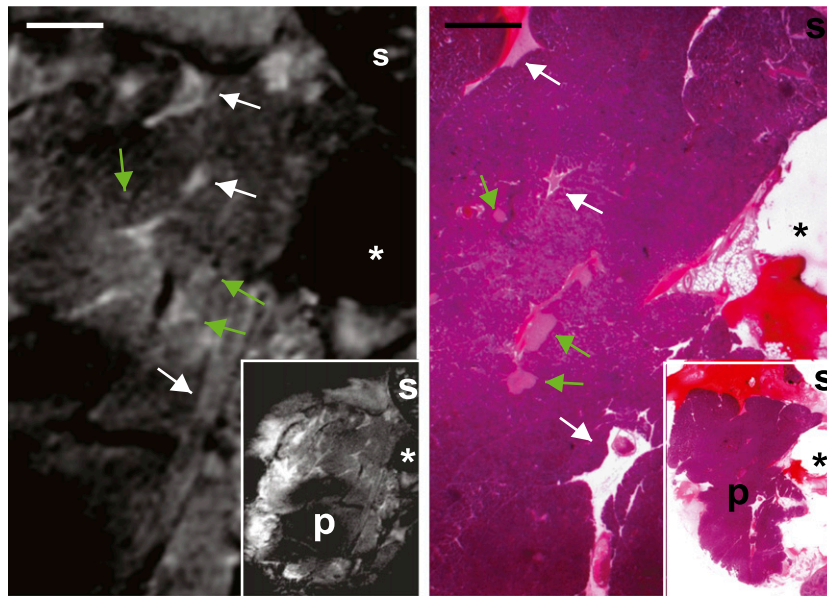


FIG. 5. MRI detects islets in situ in a living mouse. High magnifications of MR images of the exteriorized pancreas of a living, anesthetized mouse reveal a pancreatic substructure like that observed ex vivo, including the presence of elongated vessels and ducts (white arrows) and round-ovoid bodies of small size (green arrows). Histological correlation showed that these small bodies corresponded to individual pancreatic islets. Scale bar: 1 mm. Insets show low magnification views of the same pancreas. P = pancreas; s = spleen. *Position of the plastic pin that secured the pancreas. (A high-quality digital representation of this figure is available in the online issue.)

the entire exocrine tissue. This issue, however, is unlikely to limit the future translation of MRI to image the human pancreas, which features a much denser and more compact anatomy. In contrast, the future translation of MRI to the diabetes clinic faces several other problems, including the technical conditions required to obtain a sufficiently contrasted (manganese infusion) and resolvable image (high magnetic field). With regard to contrast, manganese infusion certainly raises safety questions. However, this potential problem may be overcome, and manganese-enhanced MRI is now routinely used in many clinical centers (31,32). The cation may also be replaced by alternative T1-relaxing agents (48), awaiting the availability of safer ligands to natural moieties of the β -cell membrane (19). With regard to resolution, the high magnetic field that is required, and that we used here, presently limits the approach to research on animal models until safety concerns have been adequately dealt with. However, the recent introduction of high field (3–9.4 T) equipment for whole human body MRI opens the possibility to now achieve in humans (49) a significant islet imaging, also because the manganese enhancement should be anticipated to be better than under the 14.1T conditions we tested here (50).

At any rate, the major goal of this study was to provide a first proof-of-principle that a clinically relevant imaging method can be developed to quantitatively visualize native islets in the mouse. The positive answer to this question, which is provided by our study, now opens the way to the MRI analysis of a variety of models that have been generated in this animal species, to address unanswered questions about the pathophysiology and sequence of the events that lead to diabetes.

ACKNOWLEDGMENTS

The authors' teams are supported by grants from the Swiss National Science Foundation (310000-122423, 310000-109402, 122423, CR32I3_129987); the Juvenile Diabetes Research

Foundation (40-2011-11); the European Union (BETAIMAGE 222980, Innovative Medicines Initiative for Diabetes [IMIDIA], C2008-T7); the Centre d'Imagerie BioMédicale (CIBM) of the Université de Genève (UNIGE), Healthcare Industry User Group (HIUG), Université de Lausanne (UNIL), Centre Hospitalier Universitaire Vaudois (CHUV), and Ecole Polytechnique Fédérale de Lausanne (EPFL); and the Leenaards and Jeantet Foundations.

No potential conflicts of interest relevant to this article were reported.

S.L. performed the experiments, analyzed data, and wrote the manuscript. R.I. and C.N. performed the experiments, analyzed and researched data, reviewed and edited the manuscript, and contributed to discussion. A.G. helped with the animal surgery. L.V., X.C.R.M., and R.G. contributed to discussion. P.M. wrote the manuscript.

The authors thank D. Rigo, Centre Médical Universitaire (CMU), for excellent technical assistance.

REFERENCES

1. Wild S, Roglic G, Green A, Sicree R, King H. Global prevalence of diabetes: estimates for the year 2000 and projections for 2030. *Diabetes Care* 2004; 27:1047–1053
2. Roth DJ, Jansen ED, Powers AC, Wang TG. A novel method of monitoring response to islet transplantation: bioluminescent imaging of an NF- κ B transgenic mouse model. *Transplantation* 2006;81:1185–1190
3. Speier S, Nyqvist D, Köhler M, Caicedo A, Leibiger IB, Berggren PO. Non-invasive high-resolution in vivo imaging of cell biology in the anterior chamber of the mouse eye. *Nat Protoc* 2008;3:1278–1286
4. Virostko J, Powers AC. Molecular imaging of the pancreas in small animal models. *Gastroenterology* 2009;136:407–409
5. Virostko J, Jansen ED, Powers AC. Current status of imaging pancreatic islets. *Curr Diab Rep* 2006;6:328–332
6. Weissleder R, Pittet MJ. Imaging in the era of molecular oncology. *Nature* 2008;452:580–589
7. Kherlopian AR, Song T, Duan Q, et al. A review of imaging techniques for systems biology. *BMC Syst Biol* 2008;2:74
8. Evgenov NV, Medarova Z, Dai G, Bonner-Weir S, Moore A. In vivo imaging of islet transplantation. *Nat Med* 2006;12:144–148

9. Ris F, Lepetit-Coiffe M, Meda P, et al. Assessment of human islet labeling with clinical grade iron nanoparticles prior to transplantation for graft monitoring by MRI. *Cell Transplant* 2010;19:1573–1585
10. Tai JH, Foster P, Rosales A, et al. Imaging islets labeled with magnetic nanoparticles at 1.5 Tesla. *Diabetes* 2006;55:2931–2938
11. Toso C, Vallee JP, Morel P, et al. Clinical magnetic resonance imaging of pancreatic islet grafts after iron nanoparticle labeling. *Am J Transplant* 2008;8:701–706
12. Antkowiak PF, Tersey SA, Carter JD, et al. Noninvasive assessment of pancreatic beta-cell function in vivo with manganese-enhanced magnetic resonance imaging. *Am J Physiol Endocrinol Metab* 2009;296:E573–E578
13. Denis MC, Mahmood U, Benoist C, Mathis D, Weissleder R. Imaging inflammation of the pancreatic islets in type 1 diabetes. *Proc Natl Acad Sci USA* 2004;101:12634–12639
14. Gimi B, Leoni L, Oberholzer J, et al. Functional MR microimaging of pancreatic beta-cell activation. *Cell Transplant* 2006;15:195–203
15. Ahlgren U, Gotthardt M. Approaches for imaging islets: recent advances and future prospects. *Adv Exp Med Biol* 2010;654:39–57
16. Malaisse WJ, Louchami K, Sener A. Noninvasive imaging of pancreatic beta cells. *Nat Rev Endocrinol* 2009;5:394–400
17. Biancone L, Cantaluppi V, Romanazzi GM, et al. Platelet-activating factor synthesis and response on pancreatic islet endothelial cells: relevance for islet transplantation. *Transplantation* 2006;81:511–518
18. Juang JH, Wang JJ, Shen CR, et al. Magnetic resonance imaging of transplanted mouse islets labeled with chitosan-coated superparamagnetic iron oxide nanoparticles. *Transplant Proc* 2010;42:2104–2108
19. Reiner T, Thurber G, Gaglia J, et al. Accurate measurement of pancreatic islet beta-cell mass using a second-generation fluorescent exendin-4 analog. *Proc Natl Acad Sci USA* 2011;108:12815–12820
20. Gaglia JL, Guimaraes AR, Harisinghani M, et al. Noninvasive imaging of pancreatic islet inflammation in type 1A diabetes patients. *J Clin Invest* 2011;121:442–445
21. Gotthardt M, Bleeker-Rovers CP, Boerman OC, Oyen WJ. Imaging of inflammation by PET, conventional scintigraphy, and other imaging techniques. *J Nucl Med* 2010;51:1937–1949
22. Ahlgren S, Tolmachev V. Radionuclide molecular imaging using affibody molecules. *Curr Pharm Biotechnol* 2010;11:581–589
23. van de Looij Y, Kunz N, Hüppi P, Gruetter R, Sizonenko S. Diffusion tensor echo planar imaging using surface coil transceiver with a semiadiabatic RF pulse sequence at 14.1T. *Magn Reson Med* 2011;65:732–737
24. Leoni L, Roman BB. MR imaging of pancreatic islets: tracking isolation, transplantation and function. *Curr Pharm Des* 2010;16:1582–1594
25. Nagata M, Kagawa T, Koutou D, Matsushita T, Yamazaki Y, Murase K. Measurement of manganese content in various organs in rats with or without glucose stimulation. *Radiological Phys Technol* 2011;4:7–12
26. Bock CW, Markham GD, Katz AK, Glusker JP. The arrangement of first- and second-shell water molecules in trivalent aluminum complexes: results from density functional theory and structural crystallography. *Inorg Chem* 2003;42:1538–1548
27. Bonnevie-Nielsen V, Skovgaard LT. Pancreatic islet volume distribution: direct measurement in preparations stained by perfusion in situ. *Acta Endocrinol (Copenh)* 1984;105:379–384
28. Elayat AA, el-Naggar MM, Tahir M. An immunocytochemical and morphometric study of the rat pancreatic islets. *J Anat* 1995;186:629–637
29. Hellman B, Hellerstrom C, Larsson S, Brodin S. Histochemical observations on the pancreatic islets in normal and obese-hyperglycemic mice. *Z Zellforsch Mikrosk Anat* 1961;55:235–246
30. Jo J, Choi MY, Koh DS. Size distribution of mouse Langerhans islets. *Biophys J* 2007;93:2655–2666
31. Koretsky AP, Silva AC. Manganese-enhanced magnetic resonance imaging (MEMRI). *NMR Biomed* 2004;17:527–531
32. Silva AC, Lee JH, Aoki I, Koretsky AP. Manganese-enhanced magnetic resonance imaging (MEMRI): methodological and practical considerations. *NMR Biomed* 2004;17:532–543
33. Bolaffi JL, Nowlain RE, Cruz L, Grodsky GM. Progressive damage of cultured pancreatic islets after single early exposure to streptozocin. *Diabetes* 1986;35:1027–1033
34. Bonnevie-Nielsen V, Steffes MW, Lernmark A. A major loss in islet mass and β -cell function precedes hyperglycemia in mice given multiple low doses of streptozotocin. *Diabetes* 1981;30:424–429
35. Gai W, Schott-Ohly P, Schulte im Walde S, Gleichmann H. Differential target molecules for toxicity induced by streptozotocin and alloxan in pancreatic islets of mice in vitro. *Exp Clin Endocrinol Diabetes* 2004;112:29–37
36. Gaur LK, Nepom GT, Lernmark A. Low-dose streptozotocin induces sustained hyperglycemia in *Macaca nemestrina*. *Autoimmunity* 2001;33:103–114
37. Hassan N, Janjua MZ. The optimum dose of nicotinamide for protection of pancreatic beta-cells against the cytotoxic effect of streptozotocin in albino rat. *J Ayub Med Coll Abbottabad* 2001;13:26–30
38. Li Z, Zhao L, Sandler S, Karlsson FA. Expression of pancreatic islet MHC class I, insulin, and ICA 512 tyrosine phosphatase in low-dose streptozotocin-induced diabetes in mice. *J Histochem Cytochem* 2000;48:761–767
39. McCulloch DK, Koerker DJ, Kahn SE, Bonner-Weir S, Palmer JP. Correlations of in vivo β -cell function tests with β -cell mass and pancreatic insulin content in streptozocin-administered baboons. *Diabetes* 1991;40:673–679
40. Schnedl WJ, Ferber S, Johnson JH, Newgard CB. STZ transport and cytotoxicity. Specific enhancement in GLUT2-expressing cells. *Diabetes* 1994;43:1326–1333
41. Thyssen S, Arany E, Hill DJ. Ontogeny of regeneration of beta-cells in the neonatal rat after treatment with streptozotocin. *Endocrinology* 2006;147:2346–2356
42. De Marinis YZ, Zhang E, Amisten S, et al. Enhancement of glucagon secretion in mouse and human pancreatic alpha cells by protein kinase C (PKC) involves intracellular trafficking of PKC α and PKC δ . *Diabetologia* 2010;53:717–729
43. Leitch S, Feng M, Muend S, Braiterman LT, Hubbard AL, Rao R. Vesicular distribution of secretory pathway Ca²⁺-ATPase isoform 1 and a role in manganese detoxification in liver-derived polarized cells. *Biomaterials* 2011;24:159–170
44. Reiner T, Kohler RH, Liew CW, et al. Near-infrared fluorescent probe for imaging of pancreatic beta cells. *Bioconjug Chem* 2010;21:1362–1368
45. Ris F, Morel P, Bosco D, Thierry B. Islet autotransplantation to prevent diabetes after pancreatectomy for benign disease of the pancreas. *Rev Med Suisse* 2007;3:1627–1628 [in French]
46. Schneider S. Efforts to develop methods for in vivo evaluation of the native beta-cell mass. *Diabetes Obes Metab* 2008;10(Suppl. 4):109–118
47. Souza F, Freeby M, Hultman K, et al. Current progress in non-invasive imaging of beta cell mass of the endocrine pancreas. *Curr Med Chem* 2006;13:2761–2773
48. Antkowiak PF, Mirmira RG, Epstein FH. Magnetic resonance imaging of pancreatic β -cells. In *BetaSys, Systems Biology of Regulated Exocytosis in Pancreatic β -Cells*. Booss-Bavnbek B, Klösgen B, Larsen J, Pociot F, Renström E, Eds. New York, Springer, 2011, p. 121–146
49. Atkinson IC, Sonstegard R, Pliskin NH, Thulborn KR. Vital signs and cognitive function are not affected by 23-sodium and 17-oxygen magnetic resonance imaging of the human brain at 9.4 T. *J Magn Reson Imaging* 2010;32:82–87
50. Kruk D, Kowalewski J. Field-dependent proton relaxation in aqueous solutions of some manganese(II) complexes: a new interpretation. *J Biol Inorg Chem* 2003;8:512–518